Research Article

Investigation of seismic response of topography under recorded excitation using boundary element method

Mohsen Isari[1] · Reza Tarinejad[1] · Ramtin Sobhkhiz Foumani[2] · Seyed Amir Alavi[3]

Received: 1 September 2020 / Accepted: 12 November 2020 / Published online: 19 November 2020

Abstract
Irregular topography induces non-uniform excitation in the supports of large structures such as dams and bridges. The present study employs the 3-dimensional boundary element method to achieve the seismic response of Pacoima Dam's valley and compares the numerical results with the real responses recorded during the 2001 Pacoima earthquake. The horizontal components recorded on the bottom of the valley are used as the input wave for the analysis. The time history of displacements and amplifications of different points are examined. The results revealed that the amplification factor enhanced from bottom to the top of the valley for the most frequencies. The displacement amplification ratio reached approximately 3 along the valley, suggesting the necessity for considering the non-uniform motions effects on huge structures.

Keywords Topographic effects · Boundary elements · Numerical modeling · Pacoima dam

1 Introduction

The accelerograms of an earthquake recorded in different locations can be completely different due to many reasons such as the passage effect, reflection, and refraction of seismic waves. Also, various soils beneath the supports of a structure and irregular topography of the ground can make different earthquake-induced motions. Therefore, considering non-uniform excitation for seismic analysis, particularly for structures with extensive ground contact areas can be very important to achieve real responses. However, the unavailability of earthquake records in different points of a support leads to numerous difficulties to perform non-uniform seismic analyses [1, 2]. The numerical investigations of topographic effects on the ground motion is a method to obtain non-uniform excitation and the results can be used instead of the recorded accelerograms. Most of the numerical studies have focused on 2 or 3 dimensional models with simple geometries. Among numerical methods, the boundary element method (BEM) is widely employed for the wave propagation of linear media. It is a suitable method to utilize in the infinite domains since discretization is performed only in the boundaries and the calculation efforts are significantly reduced. The present study adopted the three-dimensional time-domain boundary element method (3D TDBEM) to solve seismic responses and the results are compared to the recorded non-uniform excitation in a real valley.

Freidman and Shaw [3] began to use the 3D TDBEM to solve wave propagation problems. Niwa et al. [4] employed the TDBEM for elastodynamic problems. Mansur [5], Antes [6], and Brebbia [7] proposed time-BEM algorithms for elastodynamic problems. Karabalis and Beskos [8] and Manolis et al. [9] proposed general three-dimensional boundary element algorithms to solve elastodynamic

✉ Ramtin Sobhkhiz Foumani, Sobhkhizarman@yahoo.co.uk; Mohsen Isari, isari.mohsen@tabrizu.ac.ir; Reza Tarinejad, r_tarinejad@tabrizu.ac.ir; Seyed Amir Alavi, amir.shahamiri@yahoo.com | [1]Faculty of Civil Engineering, University of Tabriz, 29 Bahman Blvd, 51666 Tabriz, Iran. [2]Civil Engineering Department, University of Qom, Qom, Iran. [3]Civil Engineering Department, Boshehr Branch, Islamic Azad University, Boshehr, Iran.

problems based on simplified essential responses and Dirac delta essential responses, respectively. Zhao and Valliappan [10] studied the scattering of body earthquake waves due to collision with valley topography. Then, they transferred the responses in the frequency space to the time–space by the inverse transformation. Huang and Chiu [11] installed 6 accelerogram recorders in Feitsui Dam site (in Taiwan) and performed a numerical analysis to evaluate topographic resonance. Using the integral equation method in a 2-dimensional valley model and selecting the recorded accelerogram on the bottom of the valley as the input, they demonstrated that the observed and simulated records were in good agreement in terms of displacement and velocity values. Paolucci [12] studied topography amplification by a different method. They obtained the basic homogenous vibration frequency using the Rayleigh method. Then, they calculated the three-dimensional responses of some real features by spectral element approximation. Álvarez-Rubio et al. [13] solved the seismic responses of different features and suggested the capabilities of the BEM for investigating the seismic behavior of 2-dimensional valleys with irregular topographies and sedimentary beds. Kamalian et al. [14] and Kamalian et al. [15] provided the time-domain formulation of boundary elements and combined them with finite elements. Then, they used it in the seismic analyses of 2-dimensional development sites and the seismic responses of some topographic features subjected to in-plane seismic waves in homogenous and heterogeneous media. Tarinejad et al. [16] analyzed the effects of topographic amplification on valley sites using the 3-dimensional BEM. They studied the effects of some parameters on the earthquake-induced amplification, including the wave propagation frequency and angle, material properties (e.g., damping and Poisson's ratio), and the valley shape. Isari et al. [17] proposed some useful equations to calculate the time delay and coherence function of triangular valleys using the 3D TDBEM. Taghavi-Ghalesari et al. [18] studied the seismic topographic behavior subjected to body waves using the BEM. Gatmiri et al. [19] and Gatmiri et al. [20] calculated specific site spectrums in homogenous and alluvial valleys by using a hybrid software program [14, 15]. They classified the spectral homogenous valley responses by the ratio of the valley area to the wall angle. Sohrabi-Bidar et al. [21] developed the BEM to solve 3-dimensional time-domain seismic problems. They parametrically studied the seismic responses of three-dimensional arch-shaped valleys. Sohrabi-Bidar and Kamalian [22] investigated the seismic responses of 3-dimensional Gaussian-shaped hills subjected to vertical waves by using the BEM. The results indicated the wave type, site shape (including the shape ratio and dimension ratio), and wavelength are key parameters affecting the seismic behavior of the 3-dimensional hills. Panji et al. [23] and Panji et al. [24] performed topographic seismic analyses by developing the full-plane boundary element method to a half-plane BEM. Considering that the full-plane BEM requires the discretization of the flat ground and cut boundaries in distances, they developed the formulation of the full-plane BEM to a half-plane boundary element method and showed that the proposed method could be a suitable alternative to previous boundary element methods, particularly in engineering and geotechnical problems.

The present study investigates the seismic response of the Pacoima Dam site as a topographic effect-related site using the 3D TDBEM. For this purpose, a 3-dimensional model of the Pacoima Dam site is developed and the recorded accelerogram at the bottom of the valley is employed for seismic loading. The main objectives of this work are:

1. To investigate the displacement patterns of different points of the valley.
2. To evaluate the topographic amplification pattern.
3. To compare the numerical results to the real recorded excitations.

2 The numerical method

The differential equation governing the dynamic equilibrium of linear isotropic homogenous elastic media is defined as [16]:

$$\left(c_L^2 - c_T^2\right)\frac{\partial^2 u_j}{\partial x_i \partial x_j} + c_T^2 \frac{\partial^2 u_i}{\partial x_j \partial x_j} + b_i = \frac{\partial^2 u_i}{\partial t^2} \tag{1}$$

where u_i is the displacement, b_i is the body force of the medium, and c_L and c_T are the velocities of the longitudinal and transverse waves, calculated as $c_L^2 = (\lambda + 2\mu)/\rho$ and $c_T^2 = \mu/\rho$, respectively. In which λ and μ are lame constants, and ρ is the density of the medium. It should be noted that the Einstein summation convention was applied to the entire index relations of the present study. Applying the weighted-residual procedure to Eq. (1) gives the boundary integral equation governing linear isotropic homogenous elastic media as [16]:

$$c_{ij}(\xi)u_j(\xi,t) = \int_\Gamma \left\{ U_{ij}^*(x,\xi,t) \times p_j(x,t) \right\} d\Gamma - \int_\Gamma \left\{ P_{ij}^*(x,\xi,t) \times u_j(x,t) \right\} d\Gamma \tag{2}$$

where U_{ij}^* and P_{ij}^* are the fundamental solutions of the differential equation and denote the component j of the displacement and the traction of point x at time t respectively, which were obtained by applying a delta dirac concentrated load parallel to the i-axis at point ξ and time τ. Also $U_{ij}^* \otimes p_j$ and $P_{ij}^* \otimes u_j$ are the Riemann convolution integrals and c_{ij} is the known discontinuity coefficient at the point ξ, which arises from the singularity of the basic solution P_{ij}^*. c_{ij} is only the function of the boundary geometry and has the same value under both static and dynamic loading. When the medium is subject to seismic waves, the boundary integral equation changes into [16]:

$$c_{ij}(\xi) \times u_j(\xi, t) = \int_\Gamma U_{ij}^*(x,\zeta,t) \otimes p_j(x,t) \times d\Gamma - \int_\Gamma P_{ij}^*(x,\xi,t) \otimes u_j(x,t) \times d\Gamma + u_i^{inc}(\xi, t) \quad (3)$$

where u_i^{inc} is the wave-induced displacement. In homogenous topographic problems, the ground surface is stress free. Thus, Eq. (3) is rewritten as:

$$c_{ij}(\xi) \times u_j(\xi, t) = - \int_\Gamma P_{ij}^*(x,\xi,t) \otimes u_j(x,t) \times d\Gamma + u_i^{inc}(\xi, t) \quad (4)$$

for numerical solution of the problem, the boundary integral equation should be expressed such that a set of linear equations is obtained in which the boundary values are derived. To change the governing integral equation into a desirable form, first, it is separated in time and then in space. Finally, the obtained equations are shown in matrix forms as follows:

$$F_{ij1}^{N-n+1} = \int_{(n-1)\times\Delta t}^{n\times\Delta t} P_{ij}^*(x, \xi, N \times \Delta t - \tau) \times M_1(\tau) d\tau F_{ij2}^{N-n+1} = \int_{(n-1)\times\Delta t}^{n\times\Delta t} P_{ij}^*(x, \xi, N \times \Delta t - \tau) \times M2(\tau) d\tau \quad (5)$$

where F_{ij1}^{N-n+1} and F_{ij2}^{N-n+1} are the elastodynamic traction cores in the constant-location mode in a time step. Replacing Eq. (5) into the integral boundary element equations gives:

$$c_{ij}(\xi) \times u_j^N(\xi) = - \sum_{n=1}^{N} \int_\Gamma F_{ijL}^{N+1-n}(x,\xi) \times u_j^n(x) \times d\Gamma + u_i^{inc.N}(\xi) \quad (6)$$

The discretization of the variables gives the equation governing the boundary element problem as

$$c_{ij}(\xi) \times u_j^N(\xi) = - \sum_{n=1}^{N} \sum_{q=1}^{Q} U_{j\alpha}^n \times \int_{\Gamma q} F_{ijL}^{N+1-n}(x(\eta_1, \eta_2), \xi) \times \Phi_\alpha(\eta_1, \eta_2) \times |J| \times d\eta_1 d\eta_2 + u_i^{inc.N}(\xi) \quad (7)$$

where Γq is the element area, Q is the total number of boundary elements, and J is the Jacobin.

value calculated as

$$J_i = \frac{\partial x_i}{\partial n} = \frac{\partial \phi_\alpha(\eta_1, \eta_2)}{\partial n} \times X_{i\alpha} \quad (8)$$

where n is the normal vector of the element surface and $X_{i\alpha}$ is the coordinate of nodes. When Eq. (8) is written for the entire nodes, transferring the known and unknown values to the both sides of the equation and assembling the equation gives the matrix forms of the equations as

$$F^1 \times U^N = Z^N + U^{inc.N} \quad (9)$$

where Z^N is the dynamic history, the entire parameters of which are known as:

$$Z^N = \sum_{n=1}^{N-1} -F^{N+1-n} + U^n \quad (10)$$

Fundamental Solutions are obtained by a particular case of the Helmholtz decomposition, which are presented in the followings. The free-field surface displacement in a k direction in the frequency domain when the load is applied in the l direction is obtained as [16]:

$$u_{lk}^* = \frac{1}{\alpha\pi\rho c_2^2}\left[\psi\delta_{lk} - \chi r_{,l} r_{,k}\right] \quad (11)$$

where ψ and χ are defined as:

$$\psi = \frac{\exp(-k_2 r)}{r} + \left(\frac{1}{k_2^2 r^2} + \frac{1}{k_2 r}\right)\frac{\exp(-k_2 r)}{r} - \frac{c_2^2}{c_1^2}\left(\frac{1}{k_1^2 r^2} + \frac{1}{k_1 r}\right)\frac{\exp(-k_1 r)}{r}$$
$$\chi = \left(\frac{3}{k_2^2 r^2} + \frac{3}{k_2 r} + 1\right)\frac{\exp(-k_2 r)}{r} - \frac{c_2^2}{c_1^2}\left(\frac{3}{k_1^2 r^2} + \frac{3}{k_1 r} + 1\right)\frac{\exp(-k_1 r)}{r} \quad (12)$$

Hence, $\alpha = 4$; subscript (,) refers to derivation with respect to that direction; δ_{ij} represents the Kronecker delta function; r is the distance to the load point; $k_1 = \frac{i\omega}{c_1}$ and $k_2 = \frac{i\omega}{c_2}$ are compressional and shear wavenumbers, respectively.

It should be mentioned that the fundamental response of traction can be calculated based on an obtained fundamental solution for the displacement, using the relationships between stress, strain, and displacement and hence the relationships between stress and traction (Stokes law). Accordingly, the k component of the traction on a surface with unit external normal of n under a unit load in the l direction can be described as [16]:

$$p^*_{lk} = \frac{1}{\alpha\pi}[(\frac{d\psi}{dr} - \frac{1}{r}\chi)(\delta_{lk}\frac{\partial r}{\partial n} + r_{,k}n_l) - \frac{2}{r}\chi(n_k r_{,l} - 2r_{,l}r_{,k}\frac{\partial r}{\partial n}) - 2\frac{d\chi}{dr}r_{,l}r_{,k}\frac{\partial r}{\partial n} + (\frac{c_1^2}{c_2^2} - 2)(\frac{d\psi}{dr} - \frac{d\chi}{dr} - \frac{\alpha}{2r}\chi)r_{,l}n_k] \tag{13}$$

In which $d\psi/dr$ and $d\chi/dr$ are given by:

$$\frac{d\psi}{dr} = (-\frac{2}{r} - k_2 - \frac{3}{k_2 r^2} - \frac{3}{k_2^2 r^3})\frac{\exp(-k_2 r)}{r} + \frac{c_2^2}{c_1^2}(\frac{1}{r} + \frac{3}{k_1 r^2} + \frac{3}{k_1^2 r^3})\frac{\exp(-k_1 r)}{r}$$

$$\frac{d\chi}{dr} = (-\frac{4}{r} - k_2 - \frac{9}{k_2 r^2} - \frac{9}{k_2^2 r^3})\frac{\exp(-k_2 r)}{r} + \frac{c_2^2}{c_1^2}(\frac{4}{r} + k_1 + \frac{9}{k_1 r^2} + \frac{9}{k_1^2 r^3})\frac{\exp(-k_1 r)}{r} \tag{14}$$

Finally, a square matrix with the dimensions of $3Q \times 3Q$ is obtained. The unknown displacements on the boundary are found using the standard matrix solving method. The singular integrals on the main diagonal are calculated using the indirect rigid body technique, which requires closed boundaries and thus, the use of virtual elements in the half-infinite media. Based on this technique, the diagonal elements of the matrix (which contain singular integrals) are expressed with respect to off-diagonal elements (where there is no singularity). As the dynamic behavior of the traction kernel tend to be similar to the static one when the collocation and incident field nodes tend to each other, this technique can be extended to elastodynamic issues. In this study, the minimum distance between the original boundary and the new enclosing elements was set to the length of an element to ensure sufficient accuracy. The original geometry should be modeled correctly without the contribution of enclosing elements in the system of equations. The applied geometry for virtual boundary can be either circular or rectangular in shape depending on the geometry of the original boundary, which basically have no significant effect on the obtained results. [16, 21, 22, 25].

3 Case study

The records of an earthquake across the site are required to investigate the effects of non-uniform excitation on the seismic response of a dam. Such data have rarely been recorded during earthquakes in the valleys of dams, and the single recorded data are not generally enough for non-uniform analyses. Furthermore, for the rare sites with two or three points recorded data, the polynomial interpolation of the recorded points is not a suitable approach to achieve the data of the points lying between them due to the complexity of seismic wave scattering from topographic irregularities. To obtain the responses of different points of a real site, the present study built a three-dimensional topographic model of the Pacoima Dam site and used the TDBEM to calculate the seismic response. Located in Saint Gabriel Mountains, California, Pacoima Dam is an arched concrete dam with a height of 113 m and a crest length of 180 m. The body thickness of the dam varies from 3 m in the crest to 30 m at the bottom. The body of the dam is composed of 11 cantilevers with a width of 15.3 m and vertical joints between which shear keys with a depth of 30 m are embedded. An array of accelerometers was employed to record 17 displacement components (Fig. 1). Accelerometers 1–8 were placed on the dam body to evaluate the response of the structure. Accelerometers 2–4 were placed in the center of the crest to record motion in different directions. Accelerometers 1–5 were placed in the right-side one-third part and left-side one-quarter part of the crest. Like Accelerometers 1, 2, and 5, Accelerometers 6, 7, and 8 recorded the radial component at a height level of 80% of the dam.

Accelerometers 9–17 were placed near the foundation of the dam on the downstream face. Accelerometers 9–11 were installed at a height of 3 m from the bottom on the downstream face, recording different ground motion components on the bottom. Accelerometers 12–17 recorded different motion components in the joint of the dam and supports. Considering the almost north–south orientation of the dam axis, the radial and tangent horizontal components were in the east–west (along the stream direction) and north–south (perpendicular to the stream direction) directions, respectively. The high number of

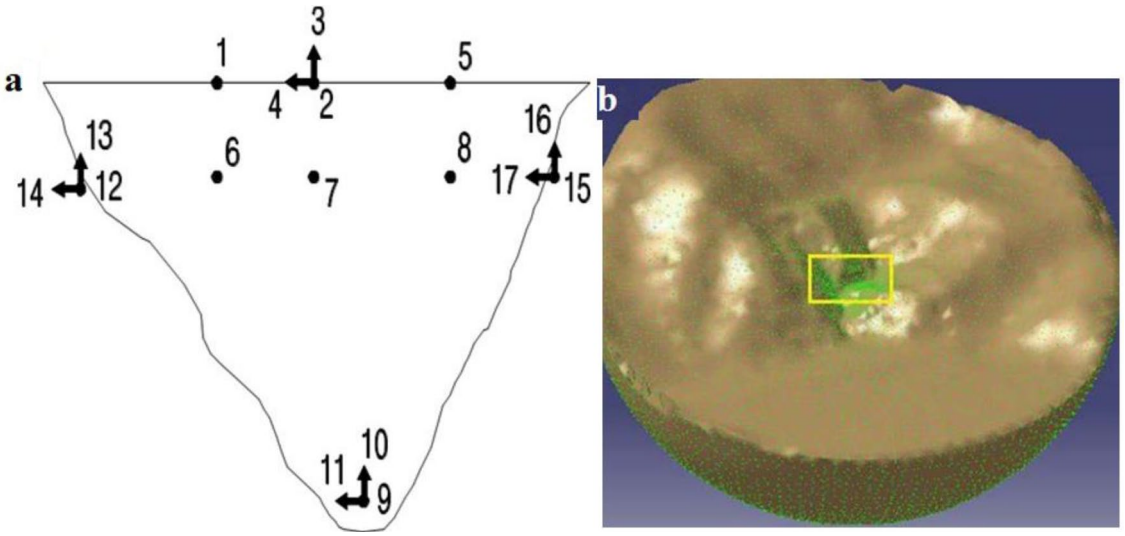

Fig. 1 **a** The cross-section of the dam and the accelerometer array locations and **b** the 3-dimensional model of the Pacoima Dam site

accelerometers in different locations on the dam body and the high number of earthquake events recorded in the site along with the relatively homogenous site of the dam provided a proper opportunity to investigate topographic effects and the real response of the dam to non-uniform support excitation during an earthquake [2].

The seismic responses of the valley under horizontal records on the bottom of the valley during the 2001 earthquake were investigated. The 2001 earthquake occurred at a distance of 6 km south of the Pacoima Dam and a depth of 9 km with a magnitude of 4.3 Richter. The storage level of the dam was reported to be 41 m below the crest during the earthquake. Also, the maximum acceleration, velocity, and displacement of the foundation were recorded to be 0.02 g, 0.9 cm/s, and 0.07 cm for the tangent components, respectively [26]. Therefore, the motion amplitude was too small to assume linear behavior during the analysis. Figure 2 shows the time-history of the recorded horizontal accelerogram in the foundation. The records of channel 9 in the length direction (i.e., *x*-direction) and those of channel 11 in the width direction (i.e., *y*-direction) were employed to study the behavior. In both cases, vertical shear wave propagation was considered. The Seismo Signal software was employed to produce excitation waves. Frequencies of above 21 Hz were excluded using a fourth-order Butterworth filter while modifying the baseline.

The BEMSA computer code [21, 22], which is based on the 3D TDBEM, was used to investigate the seismic response. The available topographic maps (i.e., the digital elevation model) were employed for the 3-dimensional modeling of the Pacoima Dam site. For this purpose, a three-dimensional model of the site was built like a semi-sphere with a radius of 5000 m from the centerpoint and 1218 eight-node elements. The shear wave velocity, density, and Poisson's ratio were considered to be 2000 m/s, 2.64 tons/m^3, and 0.25, respectively [2]. The element size of

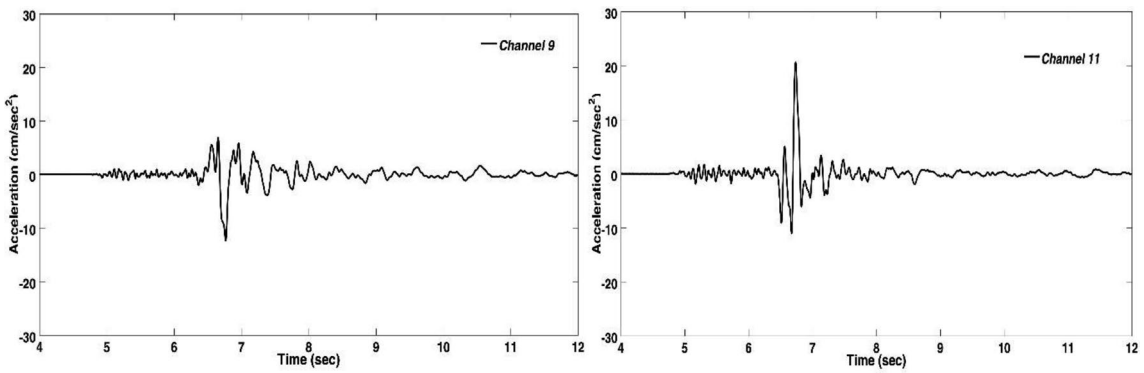

Fig. 2 The accelerogram records of the valley in channels 9 and 11 during the 2001 Pacoima Dam earthquake

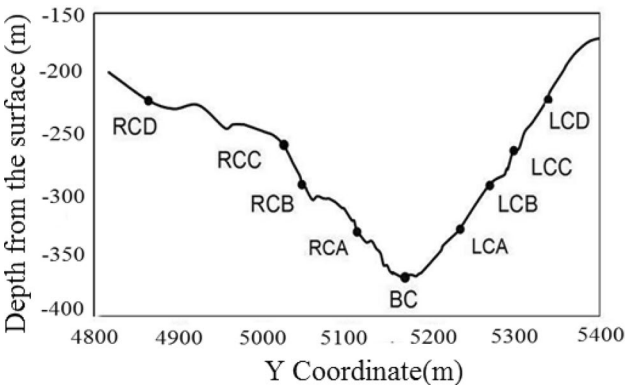

Fig. 3 The cross section of the Pacoima Dam valley and the selected points on the left and right side

the central part was about 25 m which gradually increases as moving to the sides. The observation of the displacement–time responses of different points is an interesting aspect of time-domain methods. Figure 3 depicts the selected points across the valley, which their responses are investigated. The height of the points A, B, C, and D from the bottom of the valley (BC) are 37, 66, 93, and 144 m, respectively. The Points of RCC and LCC have the same elevation as the installed accelerometers on the right and left side of the valley.

4 Evaluating the numerical results

The records of channels 9 and 11 consist of the radial and tangential components of shear waves in the *x*- and *y*-directions, respectively, were modeled in this section. Figure 4 demonstrates the time histories of displacement of 3 locations on the bottom, right and left-side of the valley, namely BC, RCC, and LCC, respectively, at a height of 80% of the dam's elevation. The results of shear wave analysis included both *x*- and *y*-directions. Figure 4 also compares the numerical seismic responses to the corresponding recorded ones. The BC records were used as the input motion. As can be seen, there was significant general consistency between the records and numerical results, with complete similarity in the displacement pattern. However, differences can be seen in the details and displacement amplitudes, which could be due to the simplified numerical model, while the experimental situation was considerably complicated. It is noteworthy that the analysis merely included the topography of the valley, while recorded accelerograms involved the interaction between the valley, Dam, and reservoir too.

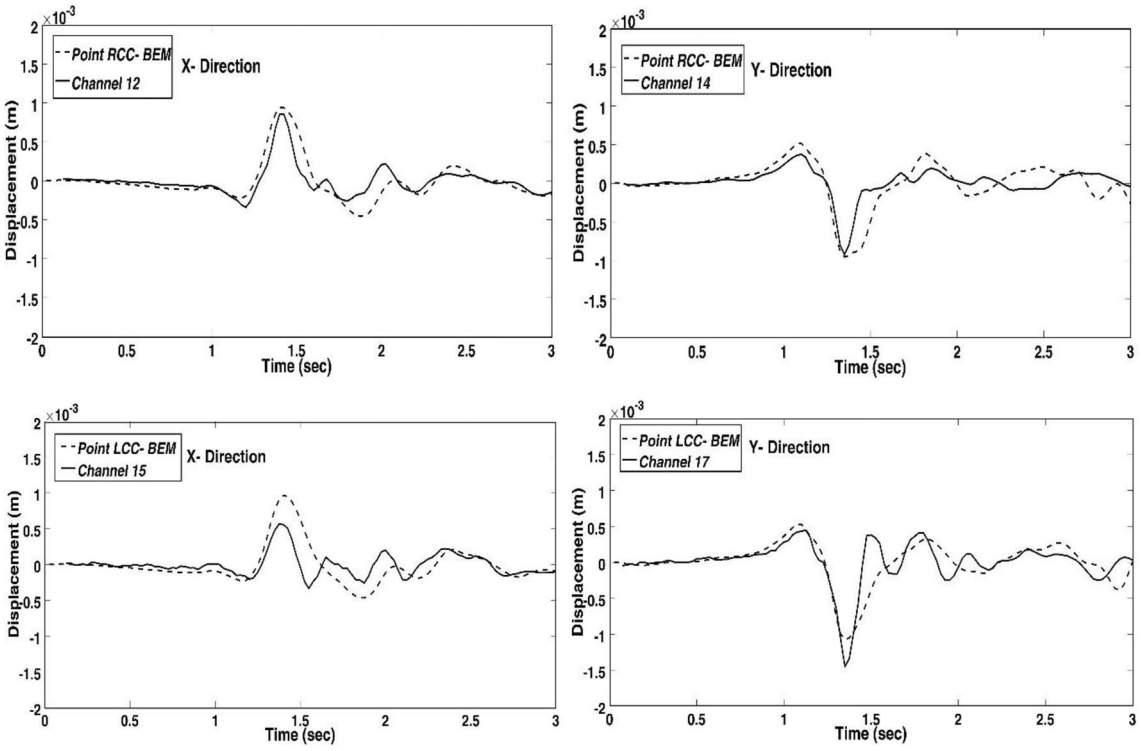

Fig. 4 The numerical displacement results of locations on the walls of the valley along with the accelerogram records of the 2001 earthquake

4.1 The shear wave seismic response in the *x*-direction

Figure 5 shows time histories of displacements for points with different heights subjected to shear waves in the *x*-direction on the both sides of the Pacoima Dam's valley. The vibration direction is along the valley, and the propagation of the shear waves was considered to be perpendicular to the dam plane. As can be seen, the displacement patterns were similar and did not considerably change as the height increased. An increase in the height unexpectedly reduced the amplitude. This could be due to the high complication of analyses under real accelerations, even though the side supports showed good consistency with the records. Moreover, the comparison of the left- and right-side locations indicate that the displacement time-histories of the same height points are different in the both sides due to the asymmetry of the valley. In general, the displacement amplitude was larger on the left side, particularly at upper heights. This could be due to the geometrical difference between the left and right walls. Table 1 provides the maximum displacement amplitudes at different heights for both sides of the valley. The maximum displacement amplitude ratio is obtained about 1.5.

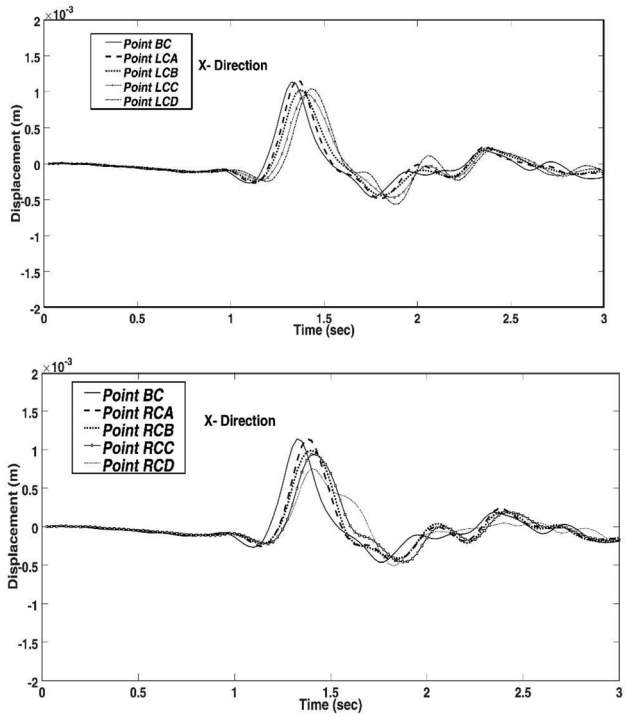

Fig. 5 The time histories of displacements for shear waves in the *x*-direction

4.2 The shear wave seismic response in the *y*-direction

Figure 6 illustrates the displacement time-histories of locations on 2 sides of the valley at different heights subjected to shear waves along the *y*-direction. The wave vibration direction is perpendicular to the valley line. Shear wave propagation was considered to occur on the plane. The displacement amplitude reduced with an increase in the height. The amplitude reduction is much larger in the *y*-direction than in the *x*-direction. Furthermore, comparing the points on two sides of the valley indicates that the displacement time-histories of points on the two sides with the same height were rather different due to the asymmetry of the valley, particularly at greater heights. In general, the displacement amplitude was larger on the left side of the valley, particularly at upper heights. Also, the differences between points at the same heights were considerably larger in the *y*-direction, suggesting the effects of the wave type and direction of wave vibration. Table 2 provides the maximum displacement values on the two sides of the valley at different heights. The maximum displacement amplitude ratio is obtained about 3.

4.3 Amplification

Figure 7 depicts the amplification diagrams obtained from the boundary element method for the left and right walls of the valley. The figure also shows the amplification curves of shear waves in both *x*- and *y*-directions. The amplification curves were plotted by calculating the ratio of the Fourier spectrum of the displacement of the points located on the right and left sides to the Fourier spectrum of the point located at the bottom (BC).

Relatively, similar amplification patterns for the shear waves in the *x*-direction are obtained for the both sides points with the same height. Large amplification factors were mostly observed around frequencies 3 and 6–8 Hz. The amplification seems to increase on both sides of the valley as the height increases, particularly at frequencies 6–8 Hz. However, the amplifications of points located

Table 1 The amplitudes of displacements corresponding to the specified points in the *x*-direction

Location	Base	A	B	C	D
Height from the bottom in the *x*-direction (m)	0	37	66	93	144
Displacement amplitudes of left-side locations (mm)	1.1	1.2	1	0.96	1
Displacement amplitudes of right-side locations (mm)	1.1	1.1	0.99	0.936	0.754

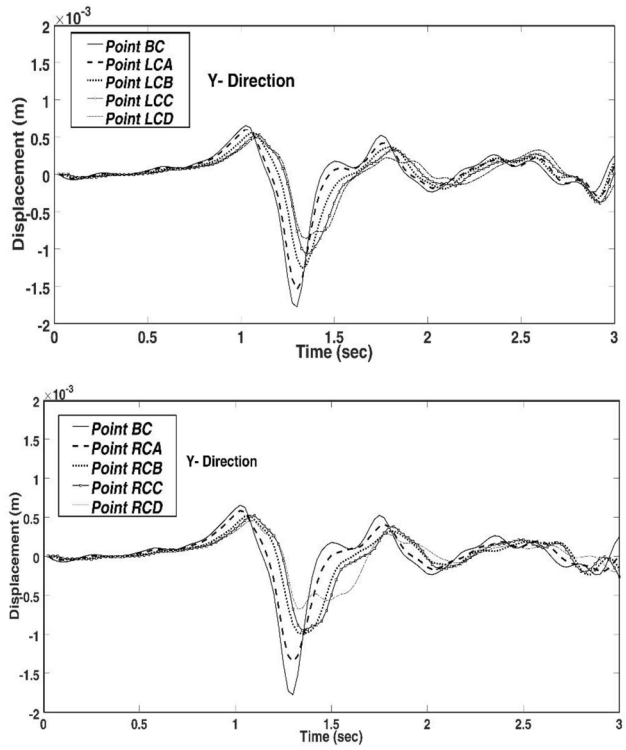

Fig. 6 The time histories of displacements in the *y*-direction

on the left side were larger than those of corresponding points with the same heights on the right side. For the shear waves in the *y*-direction, amplifications with a relatively identical pattern can be observed, except that the amplification peaks are seen at approximately 4.5 and 6–8 Hz. In this case, the amplification amplitude increased as the height increased. Compared to the shear waves in the *x*-direction, the amplification amplitudes were larger at lower frequencies for the shear waves in the *y*-direction. Like the previous case, the locations on the left side showed larger amplification than those on the right side.

Figure 8 demonstrates horizontal amplification diagrams for the 2001 Pacoima Dam earthquake records of 2 locations on the both sides from the excitation on the bottom in the radial and tangential directions. Good consistency is observed between the numerical results and the real records, particularly for the main amplification frequencies. The maximum amplification values observed at frequency ranges 3–5 and 6–8 Hz. The amplification of recorded responses is much larger than that of numerical analysis. However, considering the difference between the numerical analysis and real conditions, this inconsistency is reasonable. Also the amplification of recorded response showed new peaks at higher frequencies, which could be due to the complexity and the presence of the dam in the real condition.

5 Conclusions

This study employed the 3-dimensional boundary element method to solve the seismic response of the Pacoima Dam site. The comparison of the numerical and recorded responses of the dam site generally indicated good consistency, despite some inconsistency. It is indicated that the amplification increased at high frequencies. The results of the present study emphasized the effects of non-uniform excitation of supports in the presence of irregular topography. The results demonstrated the efficiency of the proposed method to generate non-uniform support motions using only one recorded accelerogram. The displacement amplitudes varied by approximately 1.5 and 3 times for shear waves in the *x*- and *y*-directions, respectively.

Due to the capability of BEM in combination with other numerical methods, a combined method of 3D BEM and FEM can be used to study the effects of structures such as dam on the seismic analysis results.

Table 2 The amplitudes of displacements corresponding to the specified points in the *y*-direction

Location	Base	A	B	C	D
Height from the bottom in the *x*-direction (m)	0	37	66	93	144
Displacement amplitudes of left-side locations (mm)	−1.8	−1.5	−1.3	−1.1	−0.86
Displacement amplitudes of right-side locations (mm)	−1.8	−1.4	−0.99	−0.95	−0.68

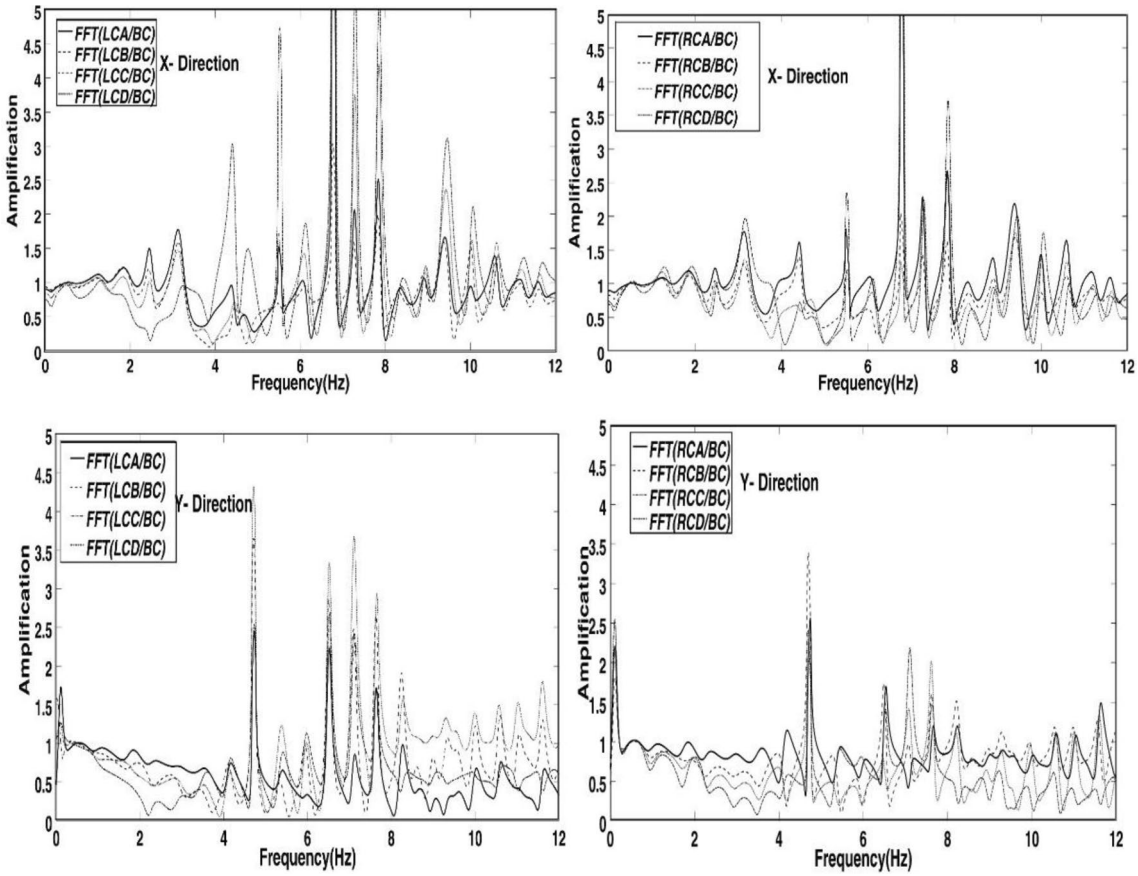

Fig. 7 The numerical amplification results

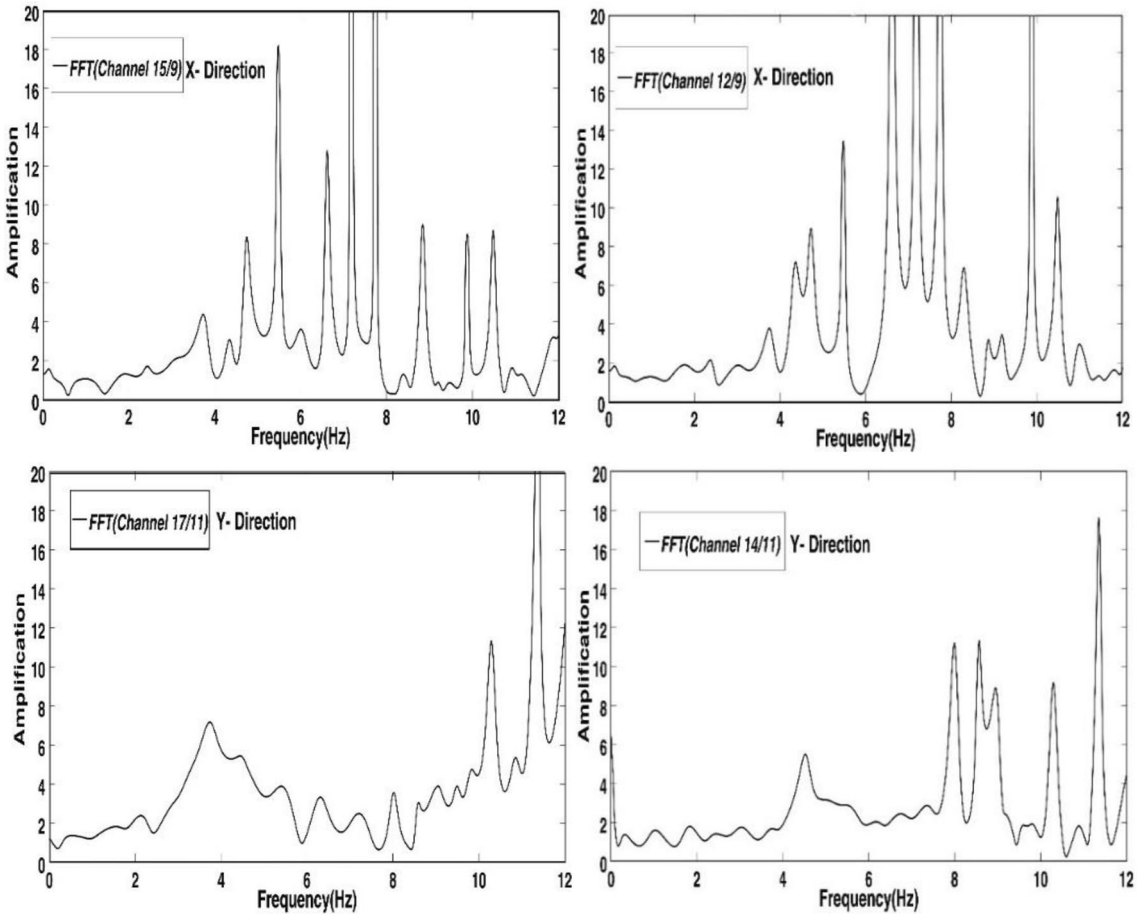

Fig. 8 The amplification records

Compliance with ethical standards

Conflict of interest We have no conflict of interest to declare.

References

1. Hariri-Ardebili MA, Mirzabozorg H (2010) Nonlinear seismic performance evaluation of concrete arch dams using endurance time method, Master of Science thesis, civil engineering. Toosi University of Technology, , Tehran
2. Tarinejad R, Fatehi R, Harichandarn RS (2013) Response of an arch dam to non-uniform excitation generated by a seismic wave scattering model. Soil Dyn Earthq Eng 52:40–54
3. Friedman MB, Shaw RP (1962) Diffraction of pulses by cylindrical obstacles of arbitrary cross-section. J Appl Mech 29:40–46
4. Niwa Y, Fukui T, Kato S, Fujiki K (1980) An application of the integral equation method to two-dimensional elastodynamics. Theory Appl Mech 28:281–290
5. Mansur WJ (1983) A time-stepping technique to solve wave propagation problems using the boundary element method. Ph.D. dissertion, Southampton University
6. Antes H (1985) A boundary element procedure for transient wave propagation in two-dimensional isotropic elastic media. Finite Elem Anal Des 1:313–322
7. Mansur WJ and Brebbia CA (1985) Transient elastodynamics. In: Brebbia CA (ed) Time-dependent and vibration problems. Topics in boundary element research, vol 2. Springer, Berlin, pp. 124–155
8. Karabalis DL, Beskos DE (1984) Dynamic response of 3-D rigid surface foundations by time domain boundary element method. Earth Eng and Struct Dyn 12:73–93
9. Manolis GD, Ahmad S, Banerjee PK (1985) Boundary element method implementation for three-dimensional elastodynamics. Developments in boundary element methods: IV. PK Banerjee, JO Watson, eds. Elsevier, London 29–63
10. Zhao, C., Valliappan, S. and Wang, Y.C. (1992) A numerical model for wave scattering problems in infinite media due to P-and SV-Wave incidences. Int J Numer Methods Eng 33(8):1661–1682
11. Huang, H.C. and Chiu, H.C. (1995) The effect of canyon topography on strong ground motion at feitsui damsite: quantitive results. Earth Eng Struc Dyn 24(7):977–990
12. Paolucci R (2002) Amplification of earthquake ground motion by steep topographic irregularities. Earth Eng and Struct Dyn 31:1831
13. Álvarez-Rubio S, José Benito J, Sánchez-Sesma FJ, Alarcón E (2005) The use of direct boundary element method for gaining insight into complex seismic site response. Comput Struct 83(10–11):821–835
14. Kamalian M, Jafari MK, Sohrabi Bidar A, Razmkhah A, Gatmiri B (2006) Time-domain two-dimensional site response analysis of

non-homogeneous topographic structures by a Hybrid FE/BE method. Soil Dyn Earthq Eng 26(8):753–765
15. Kamalian M, Gatmiri B, Sohrabi-Bidar A, Khalaj A (2007) Amplification pattern of 2D semi-sine-shaped valleys subjected to vertically propagating incident waves. Commun Numer Methods Eng 23:871–887
16. Tarinejad R, Isari M, Taghavi Ghalesari A (2019) A new boundary element solution to evaluate the geometric effects of the canyon site on the displacement response spectrum. Earthq Eng Eng Vib 18:267–284. https://doi.org/10.1007/s11803-019-0503-z
17. Isari M, Tarinejad R, Taghavi Ghalesari A, Sohrabi-Bidar A (2019) A new approach to generating non-uniform support excitation at topographic sites. Soils Found. https://doi.org/10.1016/j.sandf.2019.09.006
18. Taghavi Ghalesari A, Isari M, Tarinejad R, Sohrabi-Bidar A (2019) A procedure to predict the precise seismic response of arch dams in time domain using boundary element formulation. J R Mech Geotech Eng. https://doi.org/10.1016/j.jrmge.2018.12.014
19. Gatmiri B, Arsonb C, Nguyen KV (2008) Seismic site effects by an optimized 2D BE/FE method I: theory, numerical optimization and application to topographical irregularities. Soil Dyn Earthq Eng 28:632–645
20. Gatmiri B, Maghoul P, Arson C (2009) Site-specific spectral response of seismic movement due to geometrical and geotechnical characteristics of sites. Soil Dyn Earthq Eng 29:51–70
21. Sohrabi-Bidar A, Kamalian M, Jafari MK (2010) Seismic response of 3-D Gaussian-shaped valleys to vertically propagating incident waves. Geophys J Int 183:1429–1442
22. Sohrabi-Bidar A, Kamalian M (2013) Effects of three-dimensionality on seismic response of Gaussian-shaped hills for simple incident pulses. Soil Dyn Earthq Eng 52:1–12
23. Panji M, Kamalian M, Asgari Marnani J, Jafari MK (2013) Transient analysis of wave propagation problems by half-plane BEM. Geophys J Int 194(3):1849–1865
24. Panji M, Kamalian M, Asgari Marnani J, Jafari MK (2014) Analyzing seismic convex topographies by a half-plane time-domain BEM. Geophys J Int 197(1):591–607
25. Sohrabi-Bidar A (2008) Seismic behavior assessment of surface topographies using time domain 3D boundary elements method. Ph.D. Dissertation geophysics: Seismology. International Institute of Earthquake Engineering and Seismology
26. Alves SW (2004) Nonlinear analysis of pacoima dam with spatially non-uniform ground motion. In: Partial fulfillment of the requirements for the degree of doctor of philosophy. California Institute of Technology Pasadena, California